Control of magnetic properties of epitaxial $Mn_5Ge_3C_x$ films induced by carbon doping

A. Spiesser,[1] I. Slipukhina,[2] M.-T. Dau,[1] E. Arras,[2] V. Le Thanh,[1,*] L. Michez,[1] P. Pochet,[2,†] H. Saito,[3] S. Yuasa,[3] M. Jamet,[2] and J. Derrien[1]

[1]*Interdisciplinary Center of Nanoscience of Marseille (CINaM-CNRS), Aix-Marseille University, Campus of Luminy, Case 913, F-13288 Marseille cedex 9, France*

[2]*SP2M/INAC, CEA-UJF, F-38054 Grenoble cedex 9, France*

[3]*National Institute of Advanced Industrial Science and technology (AIST), Spintronics Research Center, Umezono 1-1-1, Central 2, Tsukuba, Ibaraki 305-8568, Japan*

(Received 9 May 2011; revised manuscript received 18 July 2011; published 3 October 2011)

We report the effects of carbon incorporation on the structural and magnetic properties of epitaxial $Mn_5Ge_3C_x$ films grown on Ge(111) by the solid phase epitaxy method. This variation of molecular beam epitaxy favors the diffusion process of carbon atoms. We show that up to a carbon molar concentration x of ~0.6–0.7, the atoms are incorporated in the interstitial sites of the Mn_5Ge_3 lattice. Such a process results in a linear increase of the Curie temperature T_C of the alloy, which can reach a value as high as ~430 K [$T_C \approx 460$ K at $M(T_C) = 0$]. Above this carbon content, T_C is found to decrease. Structural characterizations reveal that $Mn_5Ge_3C_x$ films are in perfect epitaxy when $x \leqslant 0.6$, whereas cluster formation in the grown layers is detected above that threshold. The clusters can be attributed to manganese carbide (MnC) compounds which are formed when the carbon content exceeds the saturation value of 0.6 by consuming previously deposited carbon. Theoretical calculations accurately reproduce the main trend of T_C variation as well as the cluster formation for x larger than the saturation content. In addition, we also show that after post-thermal annealing, the carbon-doped $Mn_5Ge_3C_x$ alloys remain magnetically and structurally stable up to a temperature as high as 850 °C. The results are very promising for integrating $Mn_5Ge_3C_x$ into ferromagnetic-semiconductor heterostructures, the ultimate goal being the realization of spintronic devices.

DOI: 10.1103/PhysRevB.84.165203 PACS number(s): 75.70.−i, 71.15.Mb, 75.60.Nt

I. INTRODUCTION

Spintronics is an emerging field and one of the key requirements for its development rests on obtaining spin injectors, which not only have a high Curie temperature (T_C) and a high spin polarization but also are compatible with the existing Si complementary metal-oxide semiconductor (CMOS) technology. Silicon- or germanium-based diluted ferromagnetic semiconductors (DMS) would be ideal candidates since they exhibit a natural impedance match to group-IV semiconductors. Unfortunately, $Si_{1-x}Mn_x$ alloys are not ferromagnetic and the use of $Ge_{1-x}Mn_x$ alloys would be hampered by their low T_C, which, in most cases, does not exceed 150 K.[1] As a result, to make advances in applications much effort in recent years has been devoted to epitaxial growth of ferromagnetic compounds, such as Fe_3MnSi (Ref. 2), $Fe_{1.7}Ge$ (Ref. 3) and Mn_5Ge_3.[4–8] Besides the fact that these compounds are fully compatible with Si technology, they open the possibility of spin injection via tunnel effect through the Schottky barrier without needing an oxide barrier at the interface. Among these compounds, Mn_5Ge_3 is of particular interest since in the bulk phase diagram this compound is not the most stable phase,[9] but thanks to its hexagonal structure, Mn_5Ge_3 growth on Ge(111) results in the formation of a unique epitaxial and stable phase.[4,7,8] The main drawback of Mn_5Ge_3 is its relatively low T_C (~296 K),[10] which has been shown to be enhanced by incorporating a small amount of carbon[11,12] or iron in substitutional sites.[13] The T_C enhancement with carbon doping has been attributed to Mn-Mn interactions mediated by carbon incorporated into interstitial sites of the Mn_5Ge_3 lattice.[14] However, in previous work only polycrystalline films were considered and possible diffusion (incorporation) of carbon in grain boundaries has not been taken into account, especially at high values of x (Refs. 11 and 12). Furthermore, no microscopic structural properties were provided to correlate the magnetic properties of grown films. To realize spintronic devices, ferromagnetic films of high crystalline quality and, in particular, exhibiting atomically smooth interfaces are required; this achievement was not reported for carbon-doped Mn_5Ge_3 films.

In this work, we report results of carbon doping in epitaxial Mn_5Ge_3 films grown by conventional molecular beam epitaxial (MBE) technique. It is shown that the T_C of $Mn_5Ge_3C_x$ linearly increases with x up to a saturation concentration of ~0.6–0.7; beyond that it decreases. We provide evidence that for $x \leqslant 0.6$, $Mn_5Ge_3C_x$ films are perfectly epitaxial, while for larger values of x defects and clusters appear in grown films. We have performed theoretical calculations to explain the nonmonotonous variation of T_C with x and in particular, we show that for x larger than the saturation concentration carbon atoms will no longer be inserted in Mn_5Ge_3 but will form MnC clusters, resulting in a reduction of the T_C.

II. EXPERIMENTAL SET-UP

$Mn_5Ge_3C_x$ films were grown in a MBE system by room-temperature codeposition of Mn and C on Ge substrates, followed by a thermal annealing to activate interdiffusion and phase nucleation. Note that a codeposition of three elements, Mn, C, and Ge, on a Ge substrate can be done but this requires a good control of the flux ratio to avoid a deviation from Mn_5Ge_3 stoichiometry. We have performed numerous experiments of three-element codeposition and found that with any flux deviation, in particular when the Ge flux drifts away from the value required for the alloy composition, the grown layers become highly heterogeneous due to the appearance of precipitates inside.

Standard effusion cells were used for Mn and Ge deposition; the Mn flux was measured by a quartz crystal microbalance and the Ge growth rate was deduced from measurements of reflection high-energy electron diffraction (RHEED) intensity oscillations. Carbon evaporation was carried out using a sublimation source of high-purity pyrolytic graphite (from MBE-Komponenten Company); the C concentration was estimated by combining two approaches: For each sublimation current, it was estimated from δ doping curves measured on GaAs surfaces and then corrected according to the change of Si(001) surface reconstructions from (2×1) to $c(4\times4)$ upon adsorption of a carbon submonolayer.[15] The estimated error is $\sim$10%.

$Mn_5Ge_3C_x$ growth was monitored *in situ* by a RHEED technique operating at 30 keV and Auger electron spectroscopy (AES) with a sensitivity of $\sim$1% of an atomic layer, i.e., a detection sensitivity down to 10^{12} atoms per cm^2. AES was used to control the cleanness of the substrate surface prior to Mn deposition and more importantly, to verify that the carbon doping does not change the film stoichiometry, compared to that of Mn_5Ge_3.

Structural analyses of post-grown films were performed by means of high-resolution transmission electron microscopy (HRTEM) using a JEOL 3010 microscope operating at 300 kV with a spatial resolution of 1.7 Å. HRTEM cross sections were prepared by mechanical polishing, followed by ion polishing (Gatan Precision Ion Polishing System). X-ray diffraction (XRD) characterizations were carried out using a diffractometer (Philips X'pert MPD) equipped with a copper target for Cu-$K\alpha$ radiation ($\lambda = 1.54$ Å). The angular resolution is $\sim0.01^\circ$. The magnetic properties were investigated with a superconducting quantum interference device magnetometer (SQUID) with a magnetic field applied both in the plane of the sample surface and perpendicular to it. The diamagnetic contribution, due to the Ge substrate, was subtracted from the measurements, leaving the magnetic signal of the $Mn_5Ge_3C_x$ films. More details on growth conditions and characterization techniques can be found in Refs. 7 and 8.

III. RESULTS AND DISCUSSIONS

In conventional MBE, the growth of $Mn_5Ge_3C_x$ films can, in general, proceed via two main techniques: solid phase epitaxy (SPE) and reactive deposition epitaxy (RDE). The SPE consists of codeposition at room temperature of Mn and C on Ge substrates, followed by a thermal annealing in order to activate interdiffusion. This method involves therefore two successive processes: First, interdiffusion of different species occurs and then phase nucleation takes place. In RDE, Mn and C are codeposited on substrates, which are kept at high temperatures. Depending on the substrate temperature, different phases can be formed but the phase nucleation is the main process, which occurs at the growing surface as the growth advances. Following the ideas resulting from calculations of Slipukhina *et al.*[14] in which the enhancement of T_C in $Mn_5Ge_3C_x$ results from Mn_{II}-Mn_{II} interactions mediated by carbon incorporated in octahedral voids of the hexagonal Mn_5Ge_3 cell, we have implemented the SPE technique in order to promote the carbon incorporation into interstitial sites. Indeed, since the atomic radius of carbon is almost twice as small as that of Mn and Ge, it follows that in a growth process where carbon atoms can diffuse, it becomes easier for them to be incorporated in interstitial sites. This is simply because the interstitial diffusion process is known to have the lowest activation energy. The choice of the SPE technique for studying the kinetics of the carbon incorporation in Mn_5Ge_3 seems appropriate since we found that the RDE growth leads to the formation of a random coexistence of two phases: the $Mn_5Ge_3C_x$ together with the antiferromagnetic $Mn_{11}Ge_8C_x$ phase exhibiting a Néel temperature of 150 K. This behavior will be treated in a separate paper.

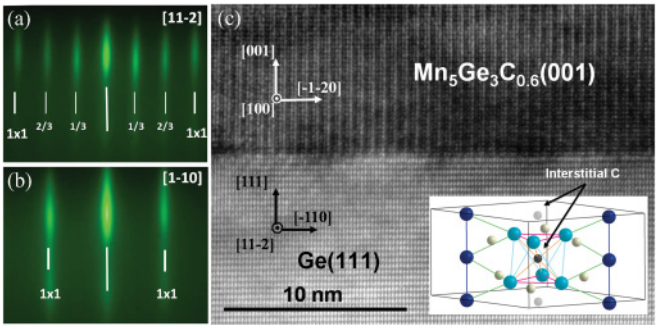

FIG. 1. (Color online) (a), (b) RHEED patterns taken along [11-2] and [1-10] azimuths of a $(\sqrt{3}\times\sqrt{3})R30^\circ$ reconstruction observed during the growth of a $Mn_5Ge_3C_x$ film with x ranging from 0.1 to 0.6. The bulklike 1×1 streaks are indicated by large white rods, and 1/3- and 2/3-ordered streaks by smaller rods. (c) High-resolution cross-sectional TEM image, showing the interface region of a $\sim$20-nm-thick $Mn_5Ge_3C_{0.6}$ film. Shown in inset is a side view of a schematic hexagonal structure of a Mn_5Ge_3 cell, illustrating two possibilities of carbon insertion in the octahedral voids without a change of the structure.

In previous works,[7,8] we have shown that in the SPE growth Mn_5Ge_3 is the unique epitaxial phase which can be formed onto Ge(111) and it is obtained by thermal annealing within the temperature range of 430–550 °C. The Mn_5Ge_3 surface is characterized by a reflection high-energy electron diffraction $(\sqrt{3}\times\sqrt{3})R30^\circ$ reconstruction, defined by the observation of 1×1 streaks along the [1-10] azimuth and 1/3- and 2/3-ordered streaks along the [11-2] azimuth. Figures 1(a) and 1(b) display typical RHEED patterns observed during $Mn_5Ge_3C_x$ growth with x ranging up to 0.6. RHEED patterns clearly exhibit a $(\sqrt{3}\times\sqrt{3})R30^\circ$ reconstruction, similar to that of Mn_5Ge_3 and appear within the same annealing temperature range of $\sim$430–550 °C.[7,8] This indicates that the carbon incorporation in Mn_5Ge_3 alters neither the surface structures nor its epitaxial relationship with Ge, i.e., the hexagonal (0001) plane of $Mn_5Ge_3C_x$ is parallel to the (111) plane of Ge. Furthermore, the observed streaky patterns also indicate that the film surface remains bidimensional within this C concentration range. We have also measured in-plane lattice parameters of $Mn_5Ge_3C_x$ films via the measurements of interdistances between (1×1) streaks and found the same value as the ones of C-free Mn_5Ge_3 films. These measurements are confirmed by x-ray diffraction analyses (not shown here), which do not reveal any shift for both (0002) and (0004) reflections of $Mn_5Ge_3C_x$, compared to Mn_5Ge_3. These structural characterizations indicate that carbon incorporated in *epitaxial* Mn_5Ge_3 films does not

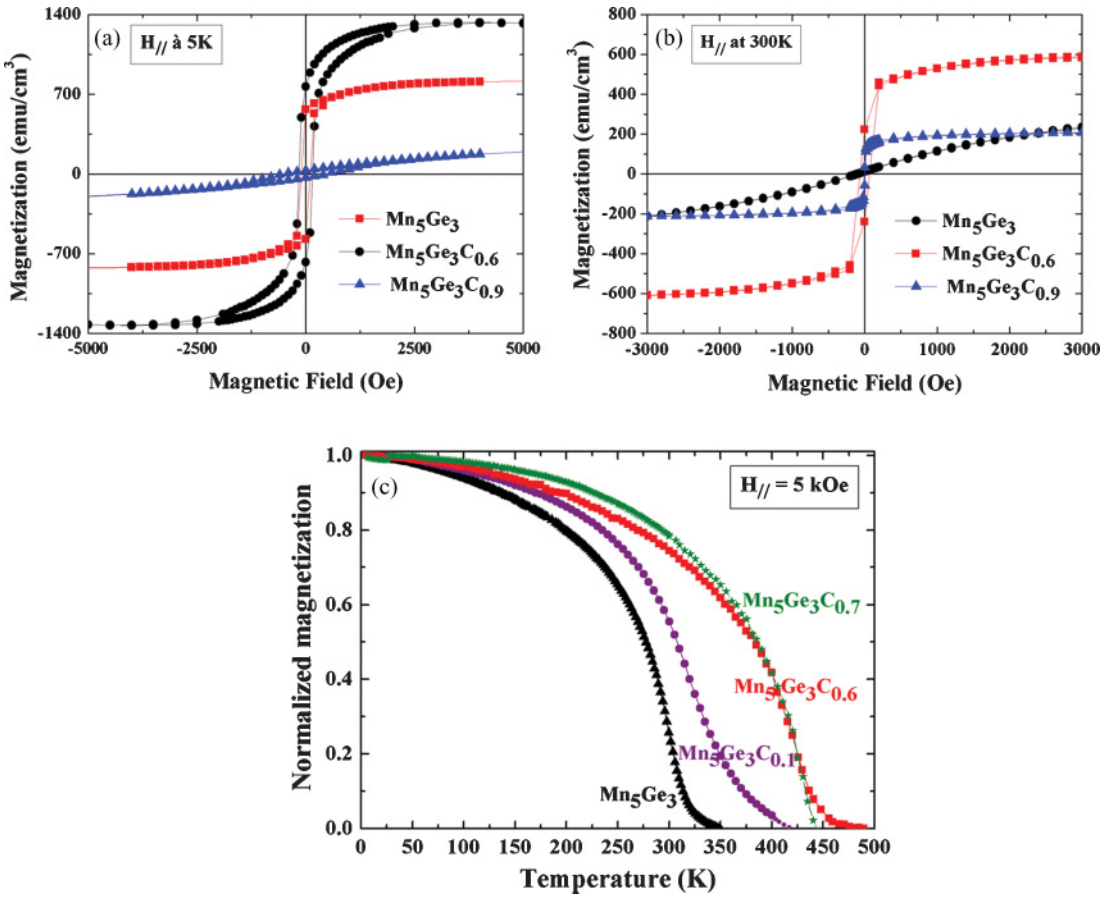

FIG. 2. (Color online) (a), (b) Hysteresis loops of different carbon-doped Mn_5Ge_3 films measured at 5 and 300 K with magnetic field applied in the film plane. (c) Evolution of normalized magnetization as a function of the temperature for various values of x in $Mn_5Ge_3C_x$ films.

provoke any lattice distortion, which is in contrast to what is observed for polycrystalline films.[11] These results also suggest that carbon is incorporated in interstitial sites of Mn_5Ge_3 since due to its small radius, substitutional carbon in *epitaxial* group-IV semiconductors should produce a local distortion around carbon atoms, giving rise to a tensile strain in the whole film.[16] It is plausible that lattice compression observed in *polycrystalline* $Mn_5Ge_3C_x$ films may result from carbon accumulation in the grain boundaries of columnar textured structures.[11]

Figure 1(c) depicts a typical cross-sectional HRTEM image of the interface region of a ∼20-nm-thick $Mn_5Ge_3C_{0.6}$ film. The image shows an extremely high-quality epitaxy of $Mn_5Ge_3C_{0.6}$ on Ge(111); no defect is detectable and the interface is atomically sharp. The transmission electron microscopy (TEM) investigation is thus in good agreement with RHEED, both indicating that for x up to 0.6, $Mn_5Ge_3C_x$ films are coherently pseudomorphic and epitaxially grown on Ge(111). Displayed in the insert is a side view of the hexagonal structure of Mn_5Ge_3, showing two possibilities of carbon insertion into the octahedral voids without provoking any change in the lattice structure.

The effects of the carbon concentration on the magnetic properties of $Mn_5Ge_3C_x$ films are depicted in Fig. 2. Figures 2(a) and 2(b) display hysteresis loops of C-free Mn_5Ge_3 and $Mn_5Ge_3C_x$ films with various C concentrations, measured by SQUID at 5 and 300 K with a magnetic field of 0.5 T applied in the film plane. At 5 K the hysteresis loops of the C-free Mn_5Ge_3 film exhibit a square shape, but become no longer ferromagnetic at 300 K [Fig. 2(b)]. At this temperature, the measured signals show a paramagnetic character. This is expected since C-free Mn_5Ge_3 is ferromagnetic only up to 296 K. For C-doped Mn_5Ge_3, measurements at 300 K clearly indicate that the materials remain ferromagnetic within the whole range of the carbon concentration. As it can be seen in Fig. 2(a), the hysteresis loops display a square shape for carbon concentrations increasing up to 0.7, but a net reduction of magnetization is observed for $x \geqslant 0.4$. It should be also noted that the average coercive field of C-doped Mn_5Ge_3 is greatly reduced: It is ∼80 Oe, compared to 300 Oe for a Mn_5Ge_3 film of the same thickness. It is worth noting that while the measurements at 300 K confirm that at $x = 0.9$ the film remains ferromagnetic, the hysteresis loops measured at 5 K display an oblate shape and show a great reduction of net magnetization. The relevance of this point will be discussed later. Note that out-of-plane measurements of hysteresis loops (not shown here) indicate that the easy axis of magnetization always lies in the film plane and the hard axis is perpendicular to it. This is attributed to the shape anisotropy effect since the thickness of all investigated samples is ∼19–20 nm.

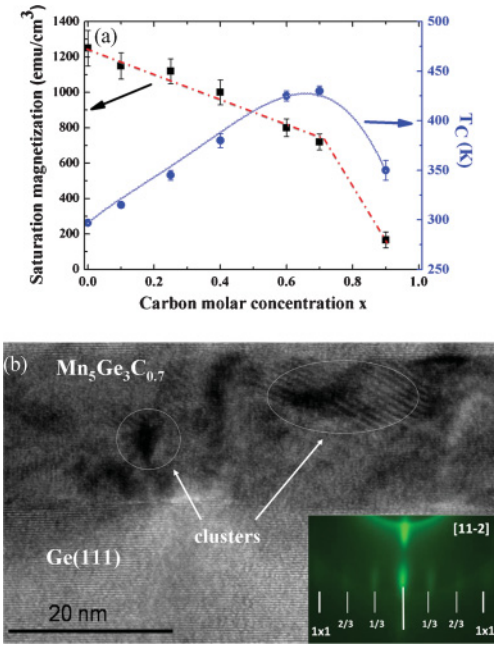

FIG. 3. (Color online) (a) Evolution of saturation magnetization M_S (left axis) and Curie temperature T_C (right axis) as a function of the carbon concentration. Note that dotted lines for M_S evolution and solid lines for carbon dependence of T_C serve as a guide to the eye. (b) Typical cross-sectional TEM image of a $Mn_5Ge_3C_{0.7}$ film, which reveals the formation of defects and clusters inside the film. Shown in inset is a RHEED pattern of the corresponding sample, indicating that three-dimensional growth occurs.

The temperature dependence of normalized magnetization of $Mn_5Ge_3C_x$ with various carbon concentrations is presented in Fig. 2(c). For comparison, we also show a curve of a C-free Mn_5Ge_3 film of the same thickness. The figure clearly indicates that addition of carbon strongly enhances magnetization of Mn_5Ge_3 and such an enhancement continuously increases with the carbon concentration up to 0.7. The T_C, measured at the inflection point of the curve M versus T, reaches a value of ∼430 K for $x = 0.6$ and 0.7. It is worth noting that for polycrystalline films, a value of the Curie temperature up to 445 K was reported for $x \sim 0.5$.[11] However, in this work the T_C was obtained from the extrapolation of the $M(T)$ data to $M(T_C) = 0$ and a similar determination of T_C of the $Mn_5Ge_3C_{0.6}$ curve shown in Fig. 2(c) gives a value up to 460 K.

We report in Fig. 3(a) the variations of T_C and of magnetization at saturation (M_S) as a function of the C concentration. The variation of T_C with x occurs in two distinct regions: T_C first linearly increases with x up to 0.6–0.7, then falls down for larger values of x. Note that this behavior is different from that previously reported for polycrystalline films. The evolution of M_S, measured at 5 K, is well correlated with the T_C variation. Saturation magnetization is found to linearly decrease with x and at $x = 0.6$–0.7, an abrupt change in the slope is observed. We note that in transition metals and their alloys, it is generally observed that magnetization at saturation increases when increasing the Curie temperature. However, as previously mentioned, in $Mn_5Ge_3C_x$ alloys the ferromagnetic enhancement results from Mn_{II}-Mn_{II} interactions mediated by carbon atoms inserted into the voids of Mn octahedra of the hexagonal structure. Consequently, carbon incorporation into Mn_5Ge_3 changes the 3d states of neighboring Mn atoms and the hybridization between the C 2p and Mn_{II} 3d states leads to a decrease of magnetization of saturation as well as magnetic moment on Mn_{II}.

These results indicate that the saturation concentration of carbon, which can be inserted into interstitial sites of the Mn_5Ge_3 lattice is around $x \sim 0.6$–0.7. From measurements of the magnetic moment at saturation and the film thickness deduced from TEM images, an average saturated Mn moment of ∼1.9 μ_B/Mn is deduced for $x = 0.7$. This value is close to the one obtained in C-implanted films[12] and with theoretical calculations,[14] but deviates from the values obtained for the sputtered films, where the highest moment of 1.1 μ_B/Mn was observed.[11]

To understand the decrease of T_C for $x \geqslant 0.7$, we show in Fig. 3(b) a typical TEM image of a sample corresponding to $x = 0.7$. In contrast to almost perfect epitaxial films observed for $x \leqslant 0.6$, the image reveals the presence of defects and in particular clusters (precipitates) in the grown film. In the insert is displayed a corresponding RHEED pattern, which indicates that although the $\sqrt{3}$ reconstruction characteristic of Mn_5Ge_3 is still present, the pattern becomes somewhat spotty, indicating that the film growth has proceeded via three-dimensional mode and the film surface is rough.

To explain the above variation of T_C in C-doped Mn_5Ge_3 films, we have performed the same two-step approach as described in Ref. 14. Moreover, in order to have a better insight into the origin and the nature of clusters, we first used a mixed density functional theory[17] and thermodynamical approach based on the reduced semigrand canonical potential similar to that already used[18] and which gives a good description of the energetics of the GeMn system.[19] Our aim is to evaluate the absolute formation energy of the carbon defects in Mn_5Ge_3, which is defined as the energy gained by the formation of the most stable phases. Thus, we have studied ten possible compounds which can be formed in three binary alloys: GeMn, GeC, and MnC.[9] The results for both Ge-C and Mn-C systems are plotted on Figs. 4(a) and 4(b), showing the evolution of the reduced grand potential versus the chemical potential differences, $\Delta_\mu^{\text{C-Mn}}$ and $\Delta_\mu^{\text{C-Ge}}$. As can be seen, our calculations reproduce well both systems: (i) Diamond C appears to be metastable by 144 meV/atom as compared to graphite C (in accordance with published results[20]), (ii) zinc blende GeC turns out to be unstable, and (iii) the relative stability of the Mn-C compounds is reproduced. After evaluating the chemical potentials μ_{Mn} and μ_{Ge} using the thermodynamic equilibriums $Mn_{11}Ge_8 \leftrightarrow Mn_5Ge_3$ and $Mn_5Ge_3 \leftrightarrow Mn_5Ge_2$, we could determine $\Delta_\mu^{\text{C-Mn}}$ and $\Delta_\mu^{\text{C-Ge}}$ in the experiments, marked by the origins in these figures.

There are four possible positions of the carbon defects in the Mn_5Ge_3 cell: The interstitial position described in Ref. 14 and three substitutional positions, Ge, Mn_I, and Mn_{II}. However, for the considered concentration $0 < x < 1$, simple defects are not isolated. We have therefore studied different concentrations and combinations of defects. First, we observe that substitutions of either Ge or Mn cost more than 2 eV, whatever the defect combinations. Second, the formation energy of the interstitial carbon is negative (−0.3 eV) up to $x = 0.5$, and becomes positive (1 eV) for $x > 0.5$. It means that

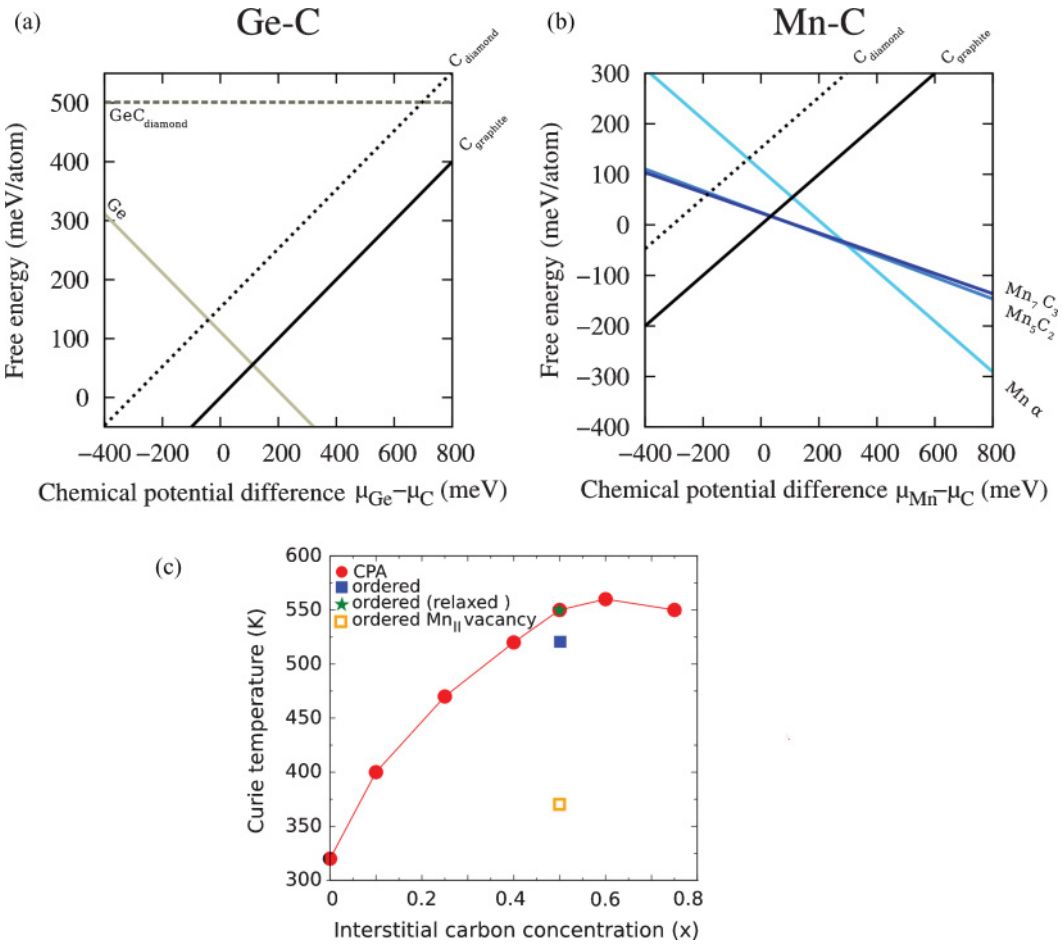

FIG. 4. (Color online) (a), (b) The reduced semigrand canonical potential as a function of the chemical potential differences $\Delta_\mu^{\text{C-Mn}}$ and $\Delta_\mu^{\text{C-Ge}}$, for different Ge-C and Mn-C compounds. At a given Δ_μ, the thermodynamically stable compound corresponds to the one with the lowest grand potential. Continuous lines correspond to the stable compounds, the dot-dashed line corresponds to the metastable ones. (c) Calculated Curie temperature as a function of the interstitial carbon concentration.

$Mn_5Ge_3C_{0.5}$ is a stable ternary alloy, and additional carbon atoms cannot be inserted into interstitial sites, but will rather form clusters, namely graphite or manganese carbides, as expected from Fig. 4(b). Since at our experimental conditions, the growth temperature does not exceed 550 °C the formation of graphite is unlikely. Thus, the formation of MnC clusters, such as Mn_7C_3 and/or Mn_5C_2, appears favorable for $x \geqslant 0.5$. This result is in agreement with the experiments which reveal that the M_S exhibits a change in the slope at $x \approx 0.5$–0.7 [Fig. 3(a)]. This also implies that magnetic characterizations appear more sensitive to the presence of defects than the structural ones. The decrease of T_C (see later) at high values of x can be therefore explained by the formation of manganese carbides, which nucleate as soon as x reaches a value of ~0.5. Upon further carbon insertion, MnC clusters tend to nucleate and in order to become stable, they should grow up to attain a certain critical size, as can be seen in Fig. 3(b). The growing process of clusters occurs in consuming a part of previously deposited carbon and/or Mn of the lattice, with the consequent formation of Mn vacancies. The formation energy of such vacancies is found to be as low as 0.5 eV.

We now return to the theoretical determination of the T_C for $Mn_5Ge_3C_x$ compounds as described in Ref. 14. Here, we go one step further by using the coherent potential approximation (CPA)[21] to treat different x concentrations without a need to use large supercells. Figure 4(c) displays the evolution of the calculated T_C with a partial occupation of the two interstitial sites by carbon up to $x = 0.8$ as we learn from the previously mentioned experimental results that full occupation of the interstitial site is not favored. We neglect structural relaxations in CPA since they were shown to have only a secondary effect on T_C. Similarly to our experimental observations, calculations nicely reproduce the T_C increase up to $x = 0.6$. This behavior confirms that the enhanced T_C mainly arises from the Mn_{II}-Mn_{II} exchange interaction mediated by interstitial carbon. However, calculations predict the highest T_C to be 550 K, which is 120 K above the experimental one. The influence of the structural relaxations cannot explain this discrepancy, since the values of T_C, calculated for both the perfect and the relaxed [blue square and green star in Fig. 4(c), respectively] ordered structure (one interstitial carbon per Mn_5Ge_3 unit cell), differ only slightly from each other and from the CPA value at $x = 0.5$. Thus, we have considered a deviation from stoichiometry in the Mn_{II} sublattice to mimic the effect of the formation of the previously mentioned MnC clusters and to check its influence on the T_C. This is done by

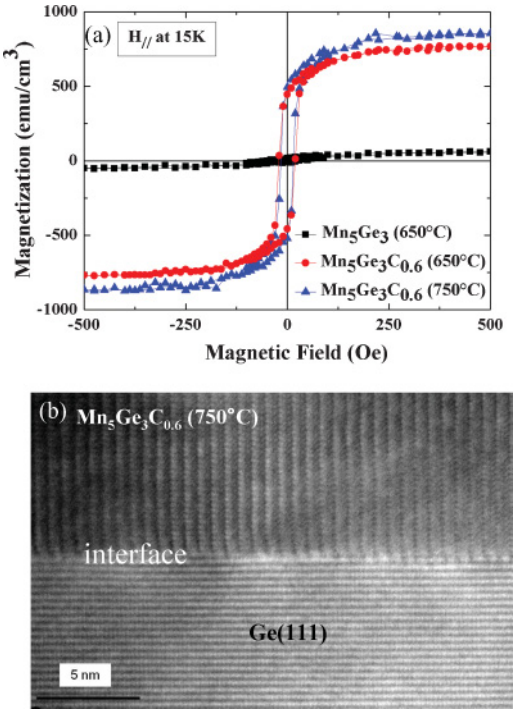

FIG. 5. (Color online) (a) Evolution of hysteresis loops measured at 15 K for a ∼20-nm-thick carbon-free Mn_5Ge_3 film annealed at 650 °C for 15 min and a $Mn_5Ge_3C_{0.6}$ film after annealing at 650 °C and 750 °C for 15 min. Note that the signal from the C-free Mn_5Ge_3 film is multiplied by a factor of 10. (b) HRTEM image of a $Mn_5Ge_3C_{0.6}$ film after annealing at 750 °C for 15 min.

considering a single vacancy at one of the six possible Mn_{II} positions (i.e., $Mn_{4.5}Ge_3C_{0.5}$ composition with almost 6 at. % of vacancies). The calculated T_C is found to reduce from 550 K down to 370 K at $x = 0.5$ (yellow square). We can thus infer that the presence of vacancies at Mn_{II} sites, which might be formed during the film growth and were not accounted for in our calculations, can explain the overestimation of the calculated T_C at $x = 0.5$ with respect to the experimental one. Moreover, this Mn-vacancy-induced reduction of the T_C is also in line with the experimentally observed strong decrease of the T_C with carbon concentration where MnC clusters are observed. It is worth noting that in the case of pure carbon precipitation conditions or carbon diffusion into grain boundaries present in polycrystalline films,[11,12] one would expect the saturation of the T_C to the value of the $Mn_5Ge_3C_{0.5}$ compound even for slightly oversaturated compounds [see Fig. 4(c)].

In view of device fabrication, an important property of materials that should be addressed is their thermal stability. Indeed, in the actual CMOS technology, the fabrication of integrated circuits requires more than 400 technological steps, among which numerous materials deposition and thermal annealing cycles are needed and sometimes at temperatures up to 700 °C. Thermal annealing of Mn_5Ge_3 and C-doped Mn_5Ge_3 films was investigated at various temperatures, ranging from 600 °C to 850 °C. Annealing was carried out just after film growth in the MBE chamber to avoid a possible surface contamination. Even if the thickness of investigated samples is relatively small (∼19–20 nm), the anneal time was chosen to be relatively long, 15 min, to insure that the system can go as close as possible to its equilibrium state. A comparison of the thermal stability of carbon-free and carbon-doped Mn_5Ge_3 films is depicted in Fig. 5(a). After annealing at 650 °C, the carbon-free Mn_5Ge_3 film exhibits an extremely weak magnetization, which indicates that its ferromagnetic character is almost lost due to the transformation from the ferromagnetic Mn_5Ge_3 phase into the antiferromagnetic $Mn_{11}Ge_8$ phase. Interestingly, the carbon-doped $Mn_5Ge_3C_{0.6}$ film does not display any change in the shape of the hysteresis loops, which remains as square as what is observed from the as-grown sample even after annealing at 750 °C. It is worth noting that after an anneal up to a temperature as high as 850 °C, the carbon-doped $Mn_5Ge_3C_{0.6}$ remains ferromagnetic although the hysteresis loops show some widening, probably due to the presence of point defects. A slight increase of magnetization with increasing the annealing temperature is also observed, which can be attributed to the out-diffusion of some carbon atoms from interstitial sites of the $Mn_5Ge_3C_{0.6}$ lattice, an inverse effect compared to that observed upon carbon doping as previously described. Structural characterizations also confirm the thermal stability of carbon-doped films, as shown in Fig. 5(b) by the HRTEM image of a $Mn_5Ge_3C_{0.6}$ film after annealing at 750 °C for 15 min. The image clearly shows atomically resolved lattice planes of both the Ge substrate and the $Mn_5Ge_3C_{0.6}$ film. Well-ordered atomic rows produced by Mn_{II} arrangement along [0001] direction similar to that of Mn_5Ge_3 are found to be perpendicular to the (111) planes of the Ge substrate.[7] Detailed analyses of the atomic distances between atomic planes confirm the epitaxial relations expected for $Mn_5Ge_3C_{0.6}$ (or Mn_5Ge_3) on Ge(111). The interface remains atomically abrupt and no modulation in the film thickness is detected. It is interesting to notice that extracted carbon atoms from interstitial sites of the $Mn_5Ge_3C_{0.6}$ lattice upon annealing do not seem to form precipitation or MnC clusters. This different behavior in the thermal stability of Mn_5Ge_3 and carbon-doped Mn_5Ge_3 can be explained as follows: From the Mn-Ge phase diagram,[9] the most stable phase is the antiferromagnetic $Mn_{11}Ge_8$ phase. Epitaxial Mn_5Ge_3 films can be stabilized on Ge(111) because of the nonequilibrium process of epitaxy and the similarity in the crystal structure between Mn_5Ge_3 and Ge(111) (the structure of Mn_5Ge_3 is hexagonal, while it is orthorhombic for $Mn_{11}Ge_8$). This means that the post-thermal annealing of grown films should bring the system progressively to a more equilibrium state, i.e., to the formation of $Mn_{11}Ge_8$. This is what we observed for carbon-free Mn_5Ge_3 films. Since the Ge content in $Mn_{11}Ge_8$ is higher than the one in Mn_5Ge_3, such a phase transformation requires a redistribution of Ge atoms inside the film or even a long-distance diffusion of Ge from the substrate. We recall that when diffusion of species occurs, the lowest-energy-cost process is mediated via interstitial sites. In C-doped Mn_5Ge_3 films, carbon atoms occupy the interstitial sites either fully or partially, depending on the carbon content. This interstitial occupation allows us to dramatically reduce or even block the Ge diffusion, making the materials thermally more stable. In other words, introducing carbon atoms into the interstitial sites of the hexagonal Mn_5Ge_3 cell not only allows the enhancement of its magnetic properties, but also prevents Ge redistribution or diffusion, making the materials more stable.

IV. CONCLUSIONS

To summarize, in an effort to insert as much carbon as possible into the octahedral voids of the hexagonal Mn_5Ge_3 cell, we have implemented the solid phase epitaxy technique, which allowed us to insert carbon up to a saturation concentration of ∼0.6–0.7. When the carbon concentration increases from 0 to the saturation value, the Curie temperature of alloys is found to linearly increase with x, reaching a value as high as 430 K. Theoretical calculations finely reproduce the main trend of the Curie temperature variation with x and in particular provide evidence that when the carbon concentration is higher than the saturation value, the formation of manganese carbide becomes thermodynamically more favorable. The formation of MnC clusters degrades the structural as well as the magnetic properties of the grown film. We have also shown that the carbon-doped $Mn_5Ge_3C_x$ alloys remain magnetically and structurally stable up to a temperature as high as 850 °C.

*lethanh@cinam.univ-mrs.fr
†pascal.pochet@cea.fr

[1] Y. D. Park, A. T. Hanbicki, S. C. Erwin, C. S. Hellberg, J. M. Sullivan, J. E. Mattson, T. F. Ambrose, A. Wilson, G. Spanos, and B. T. Jonker, Science **295**, 651 (2002).
[2] K. Hamaya, H. Itoh, O. Nakatsuka, K. Ueda, K. Yamamoto, M. Itakura, T. Taniyama, T. Ono, and M. Miyao, Phys. Rev. Lett. **102**, 137204 (2009).
[3] R. Jaafar, Y. Nehme, D. Berling, J. L. Bubendorff, A. Mehdaoui, C. Pirri, G. Garreau, and C. Uhlaq-Bouillet, Appl. Phys. Lett. **93**, 033114 (2008).
[4] C. Zeng, S. C. Erwin, L. C. Feldman, A. P. Li, R. Jin, Y. Song, J. R. Thompson, and H. H. Weitering, Appl. Phys. Lett. **83**, 5002 (2003); C. Zeng, W. Zhu, S. C. Erwin, Z. Zhang, and H. H. Weitering, Phys. Rev. B **70**, 205340 (2004).
[5] S. Picozzi, A. Continenza, and A. J. Freeman, Phys. Rev. B **70**, 235205 (2004).
[6] A. Stroppa and M. Peressi, Phys. Status Solidi A **204**, 44 (2007).
[7] S. Olive-mendez, A. Spiesser, L. A. Michez, V. Le Thanh, A. Glachant, J. Derrien, T. Devillers, A. Barski, and M. Jamet, Thin Solid Films **517**, 191 (2008).
[8] A. Spiesser, S. F. Olive-Mendez, M.-T. Dau, L. A. Michez, A. Watanabe, V. Le Thanh, A. Glachant, J. Derrien, A. Barski, and M. Jamet, Thin Solid Films **518**, S113 (2010).
[9] T. B. Massalki, in *Binary Alloy Phase Diagrams*, 2nd ed. (ASM International, Materials Park, OH, 1992), Vols. 1, 2.
[10] Y. Tawara and K. Sato, J. Phys. Soc. Jpn. **18**, 773 (1963).
[11] M. Gajdzik, C. Sürgers, M. T. Kelemen, and H. v. Löhneysen, J. Magn. Magn. Mater. **221**, 248 (2000).
[12] C. Sürgers, K. Potzger, T. Strache, W. Möller, G. Fischer, N. Joshi, and H. v. Löhneysen, Appl. Phys. Lett. **93**, 062503 (2008).
[13] T. Y. Chen, C. L. Chien, and C. Petrovic, Appl. Phys. Lett. **91**, 142505 (2007); A. Stroppa, G. Kresse, and A. Continenza, *ibid*. **93**, 092502 (2008).
[14] I. Slipukhina, E. Arras, Ph. Mavropoulos, and P. Pochet, Appl. Phys. Lett. **94**, 192505 (2009).
[15] M. Stoffel, L. Simon, J. L. Bischoff, D. Aubel, L. Kubler, and G. Castelein, Thin Solid Films **380**, 32 (2000).
[16] V. Le Thanh, C. Calmes, Y. Zheng, and D. Bouchier, Appl. Phys. Lett. **80**, 43 (2002).
[17] M. Torrent, F. Jollet, F. Bottin, G. Zerah, and X. Gonze, Comput. Mater. Sci. **42**, 337 (2008).
[18] E. Arras, I. Slipukhina, M. Torrent, D. Caliste, T. Deutsch, and P. Pochet, Appl. Phys. Lett. **96**, 231904 (2010).
[19] E. Arras, D. Caliste, T. Deutsch, F. Lançon, and P. Pochet, Phys. Rev. B **83**, 174103 (2011).
[20] A. Janotti, S.-H. Wei, and D. J. Singh, Phys. Rev. B **64**, 174107 (2001).
[21] The SPR-TB-KKR package, H. Ebert and R. Zeller, [http://olymp.cup.uni-muenchen.de/ak/ebert/SPRTB-KKR].